

# A Quantum Element Reduced Order Model

Ming-C. Cheng, Dept. of ECE, Clarkson University, Potsdam, NY 13699-5720, USA, mcheng@clarkson.edu

**Abstract**—A reduced-order model for quantum eigenvalue problems developed previously is revised and combined with the domain decomposition method to construct the quantum element method (QEM). The basic idea of the QEM is to partition a quantum domain structure into several subdomains or *elements*. Each element is projected onto a functional space using the proper orthogonal decomposition. These elements are then combined together to construct the whole domain structure. The proposed QEM has been demonstrated in 2 quantum well structures constructed with several elements. The study illustrates that the QEM is capable of offering accurate prediction of wave functions and quantum eigenenergies with a substantial reduction in the numerical degrees of freedom compared to direct numerical simulation of the Schrödinger equation.

**Keywords**—Proper orthogonal decomposition; Schrödinger equation; domain decomposition; discontinuous Galerkin; quantum wells; nanostructures

## I. INTRODUCTION

This study presents the quantum element method (QEM) that implements the quantum reduced-order model [1] based on the proper orthogonal decomposition (POD) [2]-[4] in the domain decomposition. The basic idea of the QEM is to partition a domain of a quantum eigenvalue problem into smaller *subdomains* (or elements). Each element is projected onto a functional space represented by a small set of basis functions (or modes) extracted from the POD. To construct a POD model for a large domain, the projected elements are glued together, and the interior penalty discontinuous Galerkin method [5],[6] is applied to stabilize the numerical solution and to achieve the continuity across the element interfaces. The POD is able to optimize the basis functions (or POD modes) specifically tailored to the geometry and parametric variations of the problem and can therefore substantially reduce the degrees of freedom (DoF) needed to solve the Schrödinger equation with a high accuracy.

A multi-element POD approach offers many advantages. First, to generate POD modes for a quantum eigenvalue problem, collection of wave function (WF) data in the simulation domain subjected to enough parametric variations is needed to “train” the modes [1]. In a large simulation domain especially with fine resolution, generation of POD modes of smaller subdomains is certainly more efficient. Second, domain decomposition possesses a nature advantage for parallel and/or distributed computing [7]-[10]. Finally, many quantum structures contain repeating substructures. If the selected elements appear frequently in a group of quantum structures, the quantum POD modes of these generic elements can be generated and stored in a technology library that can then be used for cost-effective simulation and design of large quantum structures. The POD approach has been successfully applied to thermal simulations of devices and integrated circuits with a high resolution [11]-[13]. It has been shown that the approach offers a reduction in numerical degrees of freedom (DoF) by 3-4 orders and 5-6 orders of magnitude in 2D and 3D domains, respectively, compared to direct numerical simulation if solution with a high resolution is needed.

## II. QUANTUM ELEMENT METHOD

### A. Formulation of the Single-Element POD Model

To generate an optimal set of modes, POD on WF data of electrons/holes for the quantum domain structure is applied based on the Fredholm equation of the second kind [2],[3],

$$\int_{\Omega} \langle \tilde{\psi}(\vec{r}) \otimes \tilde{\psi}^T(\vec{r}') \rangle \tilde{\eta}(\vec{r}') d\vec{r}' = \lambda \tilde{\eta}(\vec{r}), \quad (1)$$

where  $\otimes$  is a tensor product and  $\lambda$  is the POD eigenvalue of the data representing the mean squared WFs captured by the corresponding POD mode  $\eta$ . Once the POD modes are determined, the WF  $\psi(\vec{r})$  in the domain is given by a linear combination of these POD modes,

$$\psi(\vec{r}) = \sum_{j=1}^M a_j \eta_j(\vec{r}). \quad (2)$$

where  $M$  is the selected number of modes or the DoF for representing the WF and  $a_j$  are weighting coefficients. To derive an equation for  $\vec{a}$ , the Galerkin projection is applied to the Schrödinger equation along  $\eta_i$  in the its POD space,

$$\int_{\Omega} \nabla \eta_i(\vec{r}) \cdot \frac{\hbar^2}{2m^*} \nabla \psi(\vec{r}) d\Omega - \int_S \eta_i(\vec{r}) \frac{\hbar^2}{2m^*} \nabla \psi(\vec{r}) \cdot \hat{n} dS + \int_{\Omega} \eta_i(\vec{r}) U(\vec{r}) \psi(\vec{r}) d\Omega = E \int_{\Omega} \eta_i(\vec{r}) \psi(\vec{r}) d\Omega \quad (3)$$

where  $m^*$  is the electron/hole effective mass,  $\hbar$  the reduced Planck's constant,  $U$  the potential energy,  $E$  the quantum-state (QS) energy, and  $\hat{n}$  the outward normal vector of the boundary surface of the domain  $\Omega$ . The parametric variations are accounted for via  $U$ , which may be induced by external electric fields and/or the charge distributions in the structure.

Using (2) in (3), an equation for  $\vec{a}$  in terms of the  $M \times M$  Hamiltonian matrix  $\mathbf{H}_{\eta}$  in POD space can be derived,

$$\mathbf{H}_{\eta} \vec{a} = E_{\eta} \vec{a}, \quad (4)$$

where  $\vec{a}$  is the eigenstate vector of  $\mathbf{H}_{\eta}$  that is expressed as

$$\mathbf{H}_{\eta} = \mathbf{T}_{\eta} + \mathbf{U}_{\eta} \quad (5)$$

with the kinetic energy matrix given as

$$T_{\eta_i, j} = \int_{\Omega} \nabla \eta_i(\vec{r}) \cdot \frac{\hbar^2}{2m^*} \nabla \eta_j(\vec{r}) d\Omega \quad (6)$$

and the potential energy matrix given as

$$U_{\eta_i, j} = \int_{\Omega} \eta_i(\vec{r}) U(\vec{r}) \eta_j(\vec{r}) d\Omega. \quad (7)$$

WFs near the boundary in the single-element domain is assumed small and the surface integral vanishes. In multi-element cases, the surface integral in each element is coupled with the surrounding elements, which is presented below.

In the previous quantum POD model [1], decomposition was performed on WF data in each QS. In order to extend the QSs across multi-elements in the QEM, a global approach for all QSs is proposed. More specifically, WFs in all the selected QSs subjected to  $N_s$  different applied electric fields are collected numerically from the Schrödinger equation. Using these  $N_s$  sets of WF data in (1),  $N_s$  sets of POD

eigenvalues and eigenmodes are generated. The coefficients in (6) and (7) are then evaluated and used to solve  $\vec{a}$  in (4).

### B. Quantum Element Model

For a large structure that are partitioned into multiple elements, each element is projected to POD space using (1) represented by its POD modes. The QEM constructs the large structure using these elements and then projects the quantum eigenvalue problem of the large multi-element structure onto a POD space described by multiple sets of POD modes. To arrive at an equation for the eigenvector  $\vec{a}$  of the multi-element structure, (3) is modified to project the Schrödinger equation along the  $i$ th mode of the  $p$ th element as

$$\int_{\Omega_p} \nabla \eta_{p,i} \cdot \frac{\hbar^2}{2m_p^*} \nabla \psi_p d\Omega + \int_{\Omega_p} \eta_{p,i} U \psi_p d\Omega - \sum_{q=1, q \neq p}^{N_{el}} \int_{S_{pq}} \left[ \Delta \left( \frac{\hbar^2}{2m^*} \psi \right) \right]_{pq} \langle \nabla \eta_i \rangle_{pq} + \left\langle \frac{\hbar^2}{2m^*} \nabla \psi \right\rangle_{pq} \Delta(\eta_i)_{pq} \cdot d\vec{S} - \mu \sum_{q=1, q \neq p}^{N_{el}} \int_{S_{pq}} \Delta \left( \frac{\hbar^2}{2m^*} \psi \right) \Delta(\eta_i)_{pq} dS = E \int_{\Omega_p} \eta_{p,i} \psi_p d\Omega, \quad (8)$$

where  $N_{el}$  is the total number of elements in the domain,  $\mu$  is the penalty constant defined as  $N_{el}/dr$  with  $dr$  as the local numerical mesh size, and  $\Delta(*)_{p,q}$  and  $\langle \rangle_{p,q}$  are the difference and average in the surface integral, respectively, across the interface between the  $p$ th and  $q$ th elements. In (8), the interior penalty discontinuous Galerkin method [5],[6] is applied at the surfaces to enforce the interface continuity. For the  $p$ th element projected along its  $i$ th mode, (8) can be rewritten as

$$\sum_{j=1}^{M_p} (T_{\eta_{p,ij}} + U_{\eta_{p,ij}}) a_{p,j} + \sum_{q=1, q \neq p}^{N_{el}} \sum_{j=1}^{M_p} B_{p,pq,ij} a_{p,j} + \sum_{q=1, q \neq p}^{N_{el}} \sum_{j=1}^{M_q} B_{pq,ij} a_{q,j} = E a_{p,i}, \quad (9)$$

where  $M_p$  and  $M_q$  are the selected numbers of modes in the  $p$ th and  $q$ th elements, the interior kinetic and potential energy matrices are given in (6) and (7), the diagonal boundary kinetic energy matrix is given as

$$B_{p,pq,ij} = -\frac{1}{2} \int_{S_{pq}} \frac{\hbar^2}{2m_p^*} [(\nabla \eta_{p,i}) \eta_{p,j} + \eta_{p,i} (\nabla \eta_{p,j})] \cdot d\vec{S} + \mu \int_{S_{pq}} \frac{\hbar^2}{2m_p^*} \eta_{p,i} \eta_{p,j} dS, \quad (10)$$

and the off-diagonal boundary kinetic energy matrix is

$$B_{pq,ij} = \frac{1}{2} \int_{S_{pq}} \frac{\hbar^2}{2m_q^*} [(\nabla \eta_{p,i}) \eta_{q,j} - \eta_{p,i} (\nabla \eta_{q,j})] \cdot d\vec{S} - \mu \int_{S_{pq}} \frac{\hbar^2}{2m_q^*} \eta_{p,i} \eta_{q,j} dS. \quad (11)$$

A multi-element POD Hamiltonian matrix equation for the  $N_{el}$ -element domain can be derived from (9),

$$\begin{bmatrix} \mathbf{H}_1 & \mathbf{H}_{1,2} & \cdots & \mathbf{H}_{1,N_{el}-1} & \mathbf{H}_{1,N_{el}} \\ \mathbf{H}_{2,1} & \mathbf{H}_2 & \cdots & \mathbf{H}_{2,N_{el}-1} & \mathbf{H}_{2,N_{el}} \\ \vdots & \vdots & \ddots & \vdots & \vdots \\ \mathbf{H}_{N_{el}-1,1} & \mathbf{H}_{N_{el}-1,2} & \cdots & \mathbf{H}_{N_{el}-1} & \mathbf{H}_{N_{el}-1,N_{el}} \\ \mathbf{H}_{N_{el},1} & \mathbf{H}_{N_{el},2} & \cdots & \mathbf{H}_{N_{el},N_{el}-1} & \mathbf{H}_{N_{el}} \end{bmatrix} \begin{bmatrix} \vec{a}_1 \\ \vec{a}_2 \\ \vdots \\ \vec{a}_{N_{el}-1} \\ \vec{a}_{N_{el}} \end{bmatrix} = E \begin{bmatrix} \vec{a}_1 \\ \vec{a}_2 \\ \vdots \\ \vec{a}_{N_{el}-1} \\ \vec{a}_{N_{el}} \end{bmatrix}, \quad (12)$$

where the diagonal block matrix  $\mathbf{H}_p$  for the  $p$ th element is

$$H_{p,ij} = \sum_{j=1}^{M_p} (T_{\eta_{p,ij}} + U_{\eta_{p,ij}}) + \sum_{q=1, q \neq p}^{N_{el}} \sum_{j=1}^{M_p} B_{p,pq,ij} \quad (13)$$

and the off-diagonal block matrix  $\mathbf{H}_{pq}$  is

$$H_{pq,ij} = \sum_{j=1}^{M_q} B_{pq,ij} \quad \text{with } p \neq q. \quad (14)$$

With  $\vec{a}_p$  solved from (12) for  $p = 1$  to  $N_{el}$ , the WF in each state for the whole structure can then be constructed by combining WFs in space based on (2) over  $N_{el}$  elements. If the  $p$ th and  $q$ th elements do not neighbor each other, surface integrals in (8) vanish;  $B_{p,pq,ij} = B_{pq,ij} = 0$  and  $H_{pq,ij} = 0$ . With a large number of elements, most of matrix entries in (12) are zeros. The block matrices in (12) can be pre-evaluated from the integrals of  $\eta_{p,i}$  and  $\nabla \eta_{p,i}$ . The matrices and modes are then stored in a library for simulation/design of large quantum structures.

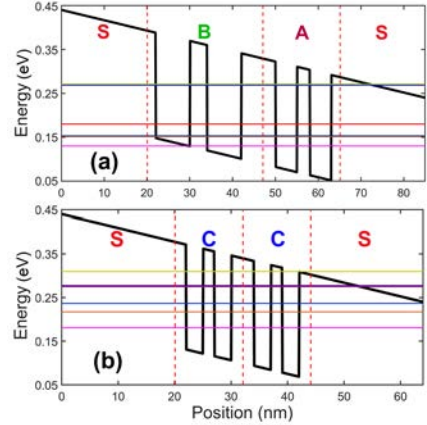


Fig. 1. Structures for generation of POD modes for each of Elements A, B, C, SC and CS. The slope of each band indicate the maximum electric field in the simulations for the data collection.

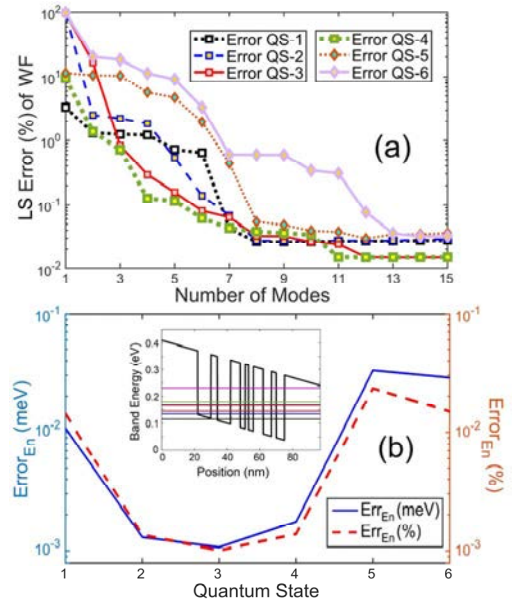


Fig. 2. (a) LS errors of WFs in Qs 1-6 derived from the 3-element POD simulations of the SB-C-AS structure at -18kV/cm. (b) The error of predicted eigenenergy with an inset showing the first 6 QS energies in the energy band at -18 kV/cm.

### III. DEMONSTRATION OF THE QEM

Two QW structures given in Fig. 1 are used to collect WF data over 6 Qs in order to generate POD modes for Elements A, B, C, SC and CS, as labeled in the band diagrams. 15 electric fields from -24 to 24 kV/cm are applied to the structure in Fig. 1(a) and from -30 to 30 kV/cm to the one in Fig. 1(b). Simulations with such setups allow each projected element to experience different boundary conditions (BCs)

induced by the adjacent elements due to electric field variations. These projected POD elements are applied to construct 2 multi-element structures to validate the QEM against detailed numerical solutions of the Schrödinger equation. The test QW structures include a 3-element structure with Elements SB, C and AS and a 7-element structure with Elements SC, B, A, B, C, A and CS.

Theoretically, the training described above allows the generated POD modes of each element to predict WFs with a high accuracy only if the element is neighbored by those encountered during the training. However, most of the elements in the test QW structures are neighbored by those not encountered in the training. As will be seen below, the generated POD modes appear to be more robust than expected. In Fig. 1(b), 2 possible sets of POD modes can be generated for Element C. The POD modes for Element C on the left are used in this study.

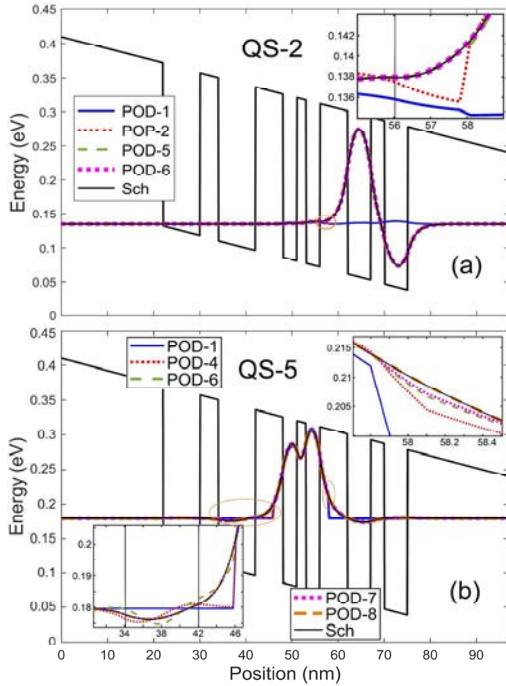


Fig. 3 Energy band diagram and WFs in QSs 2 and 5 of the 3-element structure at  $-18$  kV/cm with a different numbers of modes. The insets show the interface discontinuities influenced by the number of modes.

Using the projected POD elements, 3-element POD simulation of the SB-C-AS structure with an equal number of modes in each element and  $N_{\mu} = 20$  is performed. Compared to numerical simulation of the Schrödinger equation, errors of WFs and POD eigenenergies are illustrated in Fig. 2, and its WFs in QSs 2 and 5 are included in Fig. 3. In general, a small error of WF (near or below 2%) in each state can be reached with 2 or 3 modes for each element except for QSs 5 and 6 that require more modes to minimize the large discontinuities at interfaces between elements. With a small number of modes the discontinuity is considerably smaller in QS-2 than in QS-5. The least square (LS) error in QS-2 is thus much smaller and its error drops from 2% to 0.52% when the discontinuity near 58nm shown in the inset of Fig.3 (a) is successfully minimized with 5 modes. On the other hand, the large discontinuities in QS-5 are gradually smoothed while the number of modes increase from 4 to 6, as seen in the insets of Fig. 3(b). The LS error of the QS-5 WF in Fig. 2(a) thus gradually reduces with 4 to 6 modes, and suddenly drops from 2% to an error less than 0.1% with 7th and 8th modes included.

For the 7-element structure, simulation at an applied voltage of 0.25V across the 166nm-long QW structure (electric field  $\approx 15$  kV/cm) is performed to demonstrate effectiveness of the QEM. LS errors of the WFs in the first 14 QSs are displayed in Figs. 4(a) and 4(b). The band diagram, the first 14 eigenenergies and the errors of these eigenenergies are displayed in the insets. Some predicted WFs are illustrated in Figs. 3(a)-3(d), compared to numerical solution from the Schrödinger equation.

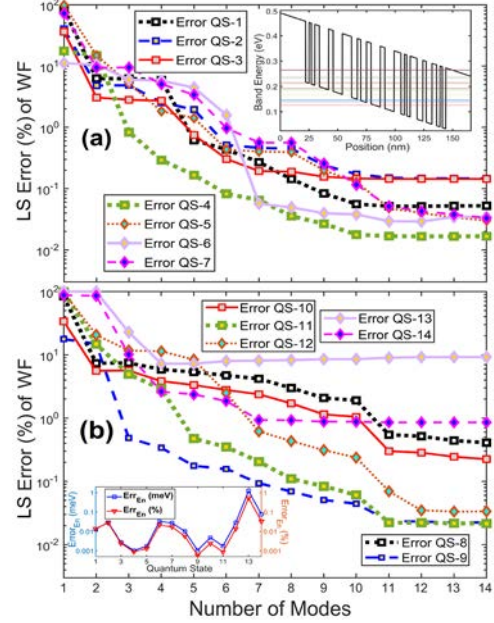


Fig. 4. LS errors of WFs in (a) QSs 1-7 and (b) QSs 8-14 derived from the 7-element POD simulation of the SC-B-A-B-C-A-CS structure at  $-15$  kV/cm. The insets display the predicted 14 QS energies in the energy band diagram in (a) and the error of the predicted eigenenergy in each QS in (b).

POD prediction of the QS energy is very accurate, as seen in the inset of Fig. 4(b), with an error less than 0.05% ( $< 0.1$  meV) for all QSs except for QS 13 whose error is 0.6% ( $< 1$  meV). Results reveal that the predicted WFs in most of states are able to reach a good accuracy with just 3 to 6 modes and the errors mostly are induced by the interface discontinuity. Once the discontinuity is suppressed using more modes, high accuracy (with an error far below 1%) can be achieved. For example, when the discontinuity in QS 1 is minimized with 5 modes (see Fig. 5(a)), a sudden drop of its error to 0.6% is found in Fig. 4(a). Except for QS 13, this is also observed in other states; some need 3 to 6 modes to minimize the discontinuity (QSs 1-7, 9 and 11) but some need 10 or 11 modes (QSs 8 and 10). Except for QSs 13 and 14, the error far below 1% can be achieved if enough modes are included. The error of the QS-14 WF stays near 1% with 7 or more modes. Unlike the other states, QS 13 appears to be an unbound state, which may not be accounted for thoroughly in the generated POD modes. As seen in Fig. 5(d), the predicted QS-13 WF is not able to reach a high accuracy and a minimum error of 7.2% is achieved with 4 modes. Fig. 4(b) shows that its error actually increases slowly as more modes are added.

The demonstrations have shown that the QEM offers a very accurate approach for the well-bounded WFs in the 2 test structures. The POD modes appear to be more *intelligent* than expected in the multi-element simulation. The POD modes are able to offer very accurate prediction even when they experience elements that were not included in the training process. However, larger errors are observed for the

unbounded WFs perhaps due to incomplete data of the unbounded WFs provided in the training process.

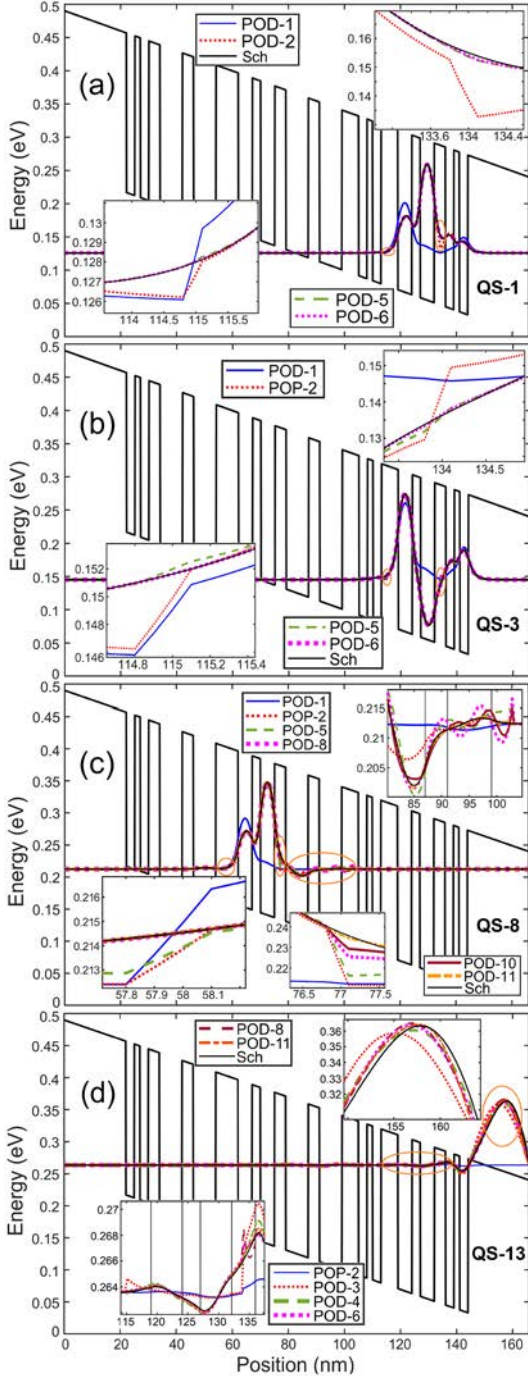


Fig. 5. Energy band diagram and WFs in Qs 1, 3, 8 and 13 of the 7-element structure at  $-15\text{ kV/cm}$  derived from the QEM with a different numbers of modes. The insets show the interface discontinuities influenced by the number of modes.

#### IV. CONCLUSIONS

The QEM proposed in this work combines the POD quantum model [1] with the domain decomposition method to offer an efficient approach for simulation of large domain structures for quantum eigenvalue problems. The approach partitions a large domain into smaller elements, each of which is projected to a POD functional space represented by a set of POD modes. The large quantum structure is then constructed using the projected POD elements. The developed QEM has been demonstrated in 2 QW structures, including a 3-element

structure with 6 QWs and a 7-element structure with 14 QWs. With the projected multi-element QW structure onto a POD space represented by the several sets of POD modes, the QEM is able to predict well-bounded WFs and QS energies with high accuracy with a small number of DoF.

This study presents the first application of the QEM. The developed approach will be useful for simulations/design of nanostructures or materials that require solution of the Schrödinger equation or Schrödinger-like equation. It is particularly useful for quantum structures with a high degree of geometrical repetition, including periodic lattice structures in materials. For simulation of a periodic structure, the general practice is to simulate a small basic element with periodic BCs, which offers a feasible computational time. In reality, there are always desired or undesired localized imperfections and/or non-uniformity in crystals or nanostructure in which periodic BCs cannot be used. To understand these types of structures, computationally intensive simulation of a large domain with a large number of basic elements, together with imperfections and/or nonuniformity, is needed. With the novel concept of the QEM, POD modes for a collection of elements, including imperfection and/or nonuniformity, can be generated first. The QEM would be able to offer accurate simulation of a large domain structure, constructed using these POD elements, to account for realistic BCs and nonuniformity at a reasonable computational time.

#### REFERENCES

- [1] M. C. Cheng, "A Reduced-Order Representation of the Schrödinger Equation," *AIP Advances*, 6, 095121, 2016.
- [2] J. L. Lumley, *Atmospheric Turbulence and Wave Propagation*, Moscow, Russia, Nauka publisher, 166 (1967).
- [3] J. L. Lumley, *Stochastic Tools in Turbulence*, Academic, New York, 1970; reprint, Dover publisher 2007.
- [4] Y. Maday and E. M. Rønquist, "A reduced-basis element method," *Comptes Rendus Math.*, 335, pp. 195–200, 2002.
- [5] D.N. Arnold, F. Brezzi, B. Cockburn, and D. Marini. "Discontinuous Galerkin methods for elliptic problems," *Lecture Notes in Comp. Sci. Eng.*, 11, pp. 89-101, 2000.
- [6] D. N. Arnold, F. Brezzi, B. Cockburn, and L. Donatella Marini. "Unified analysis of discontinuous galerkin methods for elliptic problems," *SIAM*, 39, pp. 1749-1779, 2002.
- [7] J. Mandel, "Balancing domain decomposition," *Commun. Numer. Methods Engrg.* 9 (1993) 233–241.
- [8] V. Vondrák, T. Kozubek, A. Markopoulos, Z. Dostál, "Parallel solution of contact shape optimization problems based on Total FETI domain decomposition method," *Struct. Multidiscip. Optim.* 42, 955–964, 2010.
- [9] A. Mobasher Amini, D. Dureisseix, P. Cartraud, N. Buannic, "A domain decomposition method for problems with structural heterogeneities on the interface: Application to a passenger ship," *Comput. Methods Appl. Mech. Engrg.* 198, 3452–3463, 2009.
- [10] M. Papadrakakis, G. Stavroulakis, A. Karatarakis, "A new era in scientific computing: Domain decomposition methods in hybrid CPU–GPU architectures," *Computer Methods in Applied Mechanics and Engineering*, Vol. 200, Issues 13–16, pp. 1490-1508, 2011.
- [11] W. Jia, B. Helenbrook, M. C. Cheng, "Fast Thermal Simulation of FinFET Circuits Based on a Multi-Block Reduced-Order Model", *IEEE Trans. ICs & Systems*, vol. 35, no. 7, pp. 1114-1124, 2016.
- [12] W. Jia, B. Helenbrook, M. C. Cheng, "Thermal Modeling of Multi-Fin Field Effect Transistor Structure Using Proper Orthogonal Decomposition", *IEEE Trans. Electron Devices*, Vol. 61, No. 8, pp. 2752-2759, 2014.
- [13] R. Venters, B. Helenbrook, K. Zhang, M. C. Cheng, "Proper Orthogonal Decomposition Based Thermal Modeling of Semiconductor Structures," *IEEE Trans. Electron Devices*, Vol.59, No. 11, pp. 2924-2931, 2012.